THE JOURNAL OF PHYSICAL CHEMISTRY C
A JOURNAL OF THE AMERICAN CHEMICAL SOCIETY

pubs.acs.org/JPCC

Article

Doping-Dependent Optical Response of a Hybrid Transparent Conductive Oxide/Plasmonic Medium

Maria Sygletou,* Stefania Benedetti, Alessandro di Bona, Maurizio Canepa, and Francesco Bisio

Cite This: *J. Phys. Chem. C* 2022, 126, 1881−1889

Read Online

ACCESS | Metrics & More | Article Recommendations | Supporting Information

ABSTRACT: Understanding the interaction between plasmonic nanoparticles and transparent conductive oxides is instrumental to the development of next-generation photovoltaic, optoelectronic, and energy-efficient solid-state lighting devices. We investigated the optical response of hybrid media composed of gold nanoparticles deposited on aluminum-doped zinc oxide thin films with varying doping concentration by spectroscopic ellipsometry. The dielectric functions of bare AZO were addressed first, revealing doping-induced effects such as the band gap shift and the appearance of free carriers. In the hybrid media, a blue-shift of the localized surface plasmon resonance of Au NPs as a function of increasing Al doping of the substrate was observed, ascribed to the occurrence of a charge transfer between the two materials and the doping-dependent variation of the polarizability of the substrate.

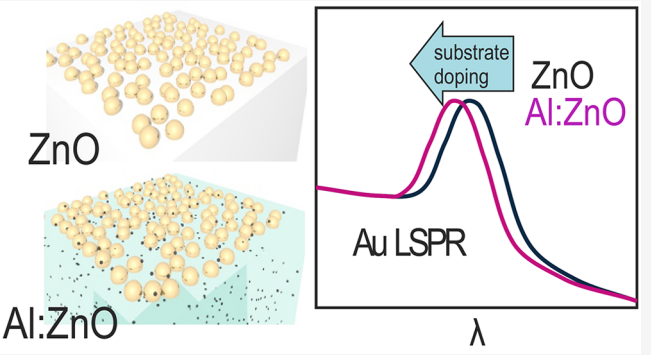

1. INTRODUCTION

Transparent conductive oxides (TCOs) have been extensively used in optoelectronics due to their visible-light optical transparency combined with low electrical resistivity[1−3] and for the possibility to realize so-called epsilon-near-zero (ENZ) materials.[4−6] Aluminum-doped ZnO (AZO) is one of such materials, based on an n-type semiconductor with direct wide-energy band gap, and cheaper than the commonly used indium−tin oxide. Aluminum doping enhances the conductivity of ZnO, making AZO suitable for applications in optoelectronic devices as a transparent conductive component and ENZ material.[7,8] AZO is cheap and easy to fabricate with various techniques, such as dc magnetron sputtering,[9] atomic layer deposition,[10] pulsed-laser deposition,[11,12] and so on. The optical properties of AZO can be tailored, to some extent, acting on the deposition parameters, like the doping level,[13,14] thickness,[15,16] or substrate temperature.[9,17]

The combination of TCOs with plasmonic nanoparticles (NPs) allows the realization of new kinds of hybrid systems[3,18−24] and metasurfaces.[25] Among the various phenomena associated with the localized surface plasmon resonance (LSPR), there is growing interest in the excitation of so-called hot electrons, i.e., energetic carriers that play a role in a variety of plasmon-induced phenomena, such as photocatalysis, photosynthesis, and more.[26,27] When NPs are in contact with TCOs, hot electrons can be injected from the NPs into the TCO by quantum tunneling through the Schottky barrier.[26,28,29] The injection of hot electrons causes a redistribution of charge carriers due to the Seebeck effect.[8,18,26,28,30] Within a NP−TCO hybrid system, not only the plasmonic NPs can modify the electro-optical properties of the TCO but also the TCO can tune the plasmon resonance of the NPs, for example, by modifying the TCO dielectric function via doping. These types of hybrid plasmonic−TCO systems in which the optical and electrical response can be controlled are extremely promising for the realization of innovative plasmo- and optoelectronics devices for ultrafast and steady-state applications.[18,25,26,28,31−46]

We based our investigations of these hybrid systems upon a very precise assessment of their dielectric characteristics (stand-alone TCO and hybrid NP/TCO), providing solid foundations for assessing the overall optical response. We addressed the optical properties of Au NPs deposited on bare and Al-doped ZnO films by means of spectroscopic ellipsometry (SE), taking the optical response of the bare TCO films as a starting point for the discussion. We covered a photon energy range broad enough to encompass both the ultraviolet interband transitions and the free-carrier range in the IR (including the ENZ region), thereby evaluating the full materials response.

Increasing the Al doping in ZnO film from 0% to 4%, we observe mainly two classes of effects, respectively, related to

Received: October 26, 2021
Revised: January 11, 2022
Published: January 25, 2022

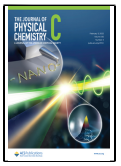

the stand-alone TCO and to the hybrid system. Among the former, we mention the blue-shift of the ZnO optical band gap[47] and the appearance of a plasma frequency in the near-IR due to the free carriers, whereas for the latter we observed a steady blue-shift of the plasmon resonance of Au NPs for increasing doping concentration (see Figure 1). Whereas to

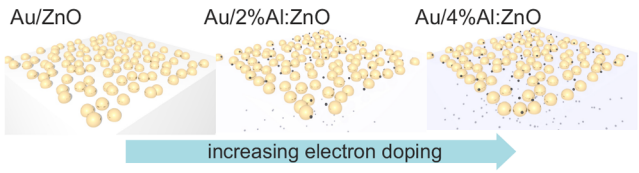

Figure 1. Schematic of the evolution of the optical properties of NPs on top of TCO films as a function of the TCO's doping level.

the first order this blue-shift can be rationalized in terms of a variation of the effective dielectric environment of the NPs, the experimental evidence suggests that charge-transfer effects between the two materials have to come into play. In this work, we provide indications that there is a charge transfer from the TCO to the metallic nanoparticles as a function of the doping concentration of the TCO by combining SE and atomic force microscopy (AFM) techniques.

2. EXPERIMENTAL SECTION

2.1. Sample Preparation. Previous studies report 4 at. % AZO as the optimum Al concentration for obtaining the highest electrical conductivity of AZO.[48,49] Above this doping level, defects have been observed in the oxide related to the depopulation of its conduction band that reduce the number of free carriers and their mobility. Based on this, AZO films with nominal content of Al = 2 and 4 at. % and bare ZnO films were deposited by magnetron sputtering on MgO (001) substrates. Before loading the substrates into the chamber, the substrates were stirred in acetone for 5 min, then ultrasonically cleaned in acetone and isopropanol in sequence for 5 min, and finally dried with nitrogen (N_2, 99.999% purity). AZO films were obtained by codeposition from a 3 in. RF magnetron source (ZnO) and a 3 in. DC magnetron source (Al) operating in confocal geometry ~15 cm far from the substrate. A constant 0.7 Å/s ZnO deposition rate was reached at a RF power of 120 W. The DC power was varied to obtain the desired doping level, in the 0−4 at. % range, defined as Al/(Al + Zn). During deposition the substrate temperature was set at 300 °C with a base pressure of 1×10^{-6} mbar in a 5×10^{-3} mbar Ar gas atmosphere. A rotating sample holder was used to obtain uniform deposition. The doping level has been checked by energy-dispersive X-ray spectroscopy and hard X-ray photoemission spectroscopy (HAXPES).[48] The control of the dopant concentration in the sputtering method with RF on ZnO target and DC on Al target was rather difficult below 1%. Furthermore, the postgrowth determination of the dopant concentration by quantitative analysis (like EDX) is limited at these low values because of the reduced amount of Al and of the vicinity of Zn and Al signals, which can hardly be deconvolved when the amount of Al is too low. For these reasons we decided to investigate and compare films with a clear dopant concentration that could be determined by EDX with a good precision. The morphology of the surface of the AZO films was examined by AFM. The AFM images of bare ZnO and AZO films of different doping levels (2% and 4%), obtained in the same deposition conditions, are shown in Figure S1 of the Supporting Information. The deposition parameters were set after a parametric study for the optimization of the surface roughness of bare ZnO films on MgO substrates. Indicative microscopy images of this study are presented in Figure S2. The root-mean-square surface roughness of the bare ZnO film was around 1.5 nm, and it increased up to 2.2 nm for 2 at. % AZO and up to 2.7 nm for 4 at. % AZO film.

Au NPs were deposited on AZO by molecular beam epitaxy: 3 nm of Au deposited at normal incidence angle by molecular beam epitaxy at $p \approx 10^{-9}$ mbar on the AZO/MgO substrate in a dedicated chamber. The Au/AZO/MgO system was annealed at 400 °C in the deposition chamber, resulting in the formation of isolated NPs, according to AFM. The AFM image in Figure 2 shows the surface morphology of Au NPs

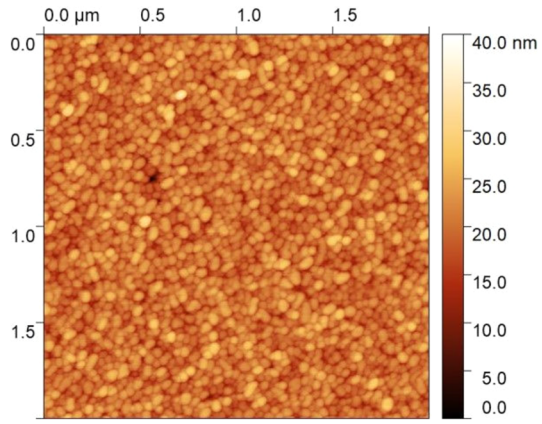

Figure 2. AFM image of Au NPs deposited on top of 2 at. % AZO film grown on MgO substrate.

deposited on top of 2 at. % AZO film. No significant differences are observed on the Au NPs grown on the different substrates (see Figure S1, bottom). The mean size of the NPs was around 20−25 nm.

2.2. Spectroscopic Ellipsometry (SE). SE is a very sensitive and nondestructive technique for investigating the optical response of materials, successfully applied to various TCOs and other systems of complex nanoscale morphology.[9,13−15,17,50−52] It was performed by means of a J.A. Woollam V-VASE ellipsometer (0.49−5.05 eV range, incidence angles of 60° and 65°), under ambient conditions. SE is based on the measurement of the variation of the polarization state of light reflected at non-normal incidence off the sample surface; it yields the so-called ellipsometry angles $\Psi(\lambda)$ and $\Delta(\lambda)$, defined by the equation $r_p/r_s = \tan \Psi e^{i\Delta}$, where $r_{p(s)}$ are the Fresnel reflection coefficients for p(s)-polarized radiation.[53−55]

From the optical point of view, the system was modeled as a stack of dielectric layers, each characterized by its thickness and complex dielectric function, representing the various physical layers of the samples. The optical response of the system was calculated assuming Fresnel boundary conditions at the interface between the layers. The thickness of the films was independently measured by using profilometry to provide a first-order estimation for SE modeling. In addition, the transmission spectrum of 2 at. % AZO films, deposited on a two-side polished MgO substrate, was measured in the 1.00−

https://doi.org/10.1021/acs.jpcc.1c07567
J. Phys. Chem. C 2022, 126, 1881−1889

5.05 eV photon energy range to provide a straightforward evidence for the LSPR response of Au NPs.

For the SE modeling, we used WVASE software (J.A. Woollam, Co.), allowing a thorough characterization of the optical constants, film thickness, and roughness of the materials involved. Bottom to top, the model included (i) a semi-infinite polished MgO(001) substrate, (ii) the AZO film, (iii) a roughness layer, and (iv) an effective layer representative of the Au NPs deposited on the AZO surface. For modeling the optical properties of AZO we resorted to a superposition of Lorentz, Lorentz−Gaussian, and so-called PSEMI oscillators[56,57] along with a Drude-type contribution for representing the doping-induced free carriers. PSEMI oscillators are parametrized functions widely employed for modeling the optical response of crystalline semiconductors. The oscillator parameters of the undoped ZnO and the AZO layer as well as the thickness of all the optical layers were carefully fitted to achieve the best agreement between the experimental data and the simulated SE spectra. PSEMI oscillators were also employed for the effective modeling of the optical properties of the Au−NP layer on top of the TCO films. All the layers in the model were isotropic. The existence of any in-plane anisotropy was ruled out by azimuthal-angle-dependent measurements, while the good fitting of the isotropic model applied to measurements collected at different angles of incidence suggests that out-of-plane anisotropy is weak or negligible.

3. RESULTS AND DISCUSSION

3.1. Optical Properties of AZO Films. In Figure 3, the ellipsometry spectra Ψ and Δ of bare and Al-doped (2 and 4 at. %) ZnO films, acquired with incidence angle of 65°, are presented in the same graph for comparison. Fits with a mean-squared error (MSE) of 2.39, 4.65, and 4.74 were obtained for bare, 2 at. % doped, and 4 at. % doped film and Al-doped ZnO films, respectively. Additional spectra at different incidence angles are shown in Figure S3 along with the best fits obtained in correspondence of the dielectric functions reported in Figure 4 and of the morphological parameters (film thickness and roughness) reported below. The Ψ and Δ spectra of undoped ZnO show prominent features close to the band gap region, in the near-UV, and are relatively featureless in the visible−IR regions. Doped films exhibit a clear evolution of the spectral features in the near-UV region and appearance of characteristic features in the near-IR region around 0.7 eV, which are attributed to the bulk-plasmon resonance of the AZO films. The origin and evolution of all these features can be understood by looking at the complex dielectric function ε of the AZO films extracted from these data and presented in Figure 4 (the corresponding complex refractive index (n, k) are reported in Figure S4). The dielectric function of the AZO films is the physical quantity that carries all the information about the materials' response (band gap, polarizability, bulk plasmon resonance, and Drude contribution), eliminating the thickness dependence.

In Figures 4a and 4b we report the real (ε_1) and the imaginary (ε_2) part of the dielectric functions of the AZO films as extracted from ellipsometry data. A few things stand out from these data. Starting from the UV range, the optical band gap was 3.27 eV for pure ZnO films, increasing as a function of doping due to the Burstein−Moss effect, upon which the absorption edge is pushed to higher energies because of the occupation of the bottom of the conduction band.[47] In Figure 4c we report the calculation of the band gap values by means of a Tauc plot. Upon 2% Al doping the band gap of ZnO increases up to 3.79 eV, while the further increase of the doping pushes the band gap to only slightly higher values (3.84 eV). This blue-shift agrees well with the corresponding blue-shift of the UV features in the SE spectra as a function of doping in Figure 3 (top). The marked excitonic peak at the band gap edge of ZnO is gradually damped as doping increases.

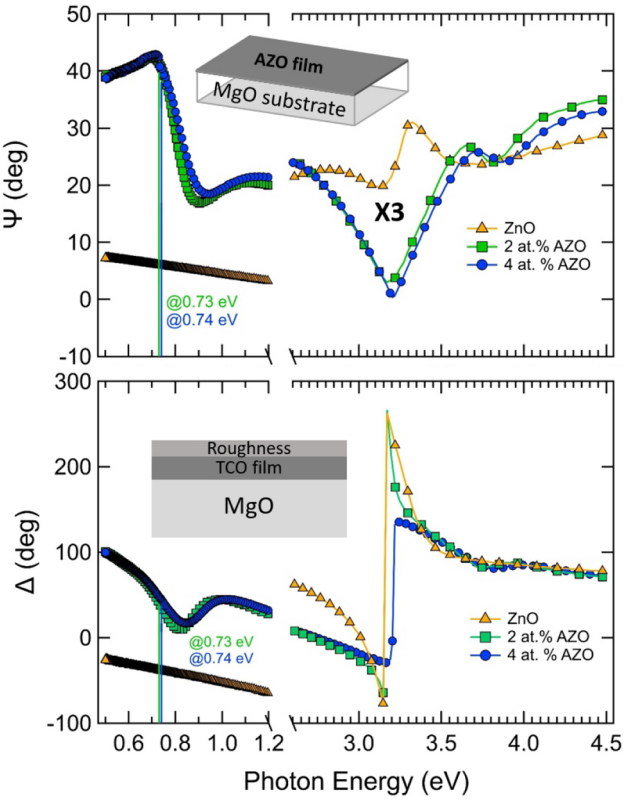

Figure 3. Ψ (top) and Δ (bottom) spectra of ZnO (triangles), 2 at. % AZO (squares), and 4 at. % AZO (circles) films, grown on MgO substrates, acquired with an incidence angle of 65°. The Ψ spectra above 2.6 eV have been multiplied by a factor of 3 for the sake of clarity. The solid lines in both spectra indicate the plasma frequency for 2 at. % AZO (green) and 4 at. % AZO (blue line). The inset on the top image is a representative scheme of the samples under study (AZO film/MgO substrate, one side polished). The inset on the bottom image is a representative scheme of the model used for the fit of the experimental ellipsometry data.

In the visible region (approximately from 2 to 3 eV) the optical absorption approaches zero as expected for TCO systems. The spectral fingerprint of some defect state in the band gap is observable as a deviation from perfect transparency in the visible range.

In the near-IR the free-carrier contribution is apparent, with the appearance of a screened plasma frequency at 0.73 eV (0.74 eV) for 2 at. % AZO (4 at. % AZO). At the plasma frequency, ε_2 values below 0.5 are observed, indicative of high-quality ENZ behavior. The crossing of the plasma frequency is actually responsible for the sharp features observed in the SE spectra of Figure 3, where the dip in the Δ and the sharp rise in Ψ are the fingerprints of the crossover from dielectric to metallic behavior.[58] We point out that the appearance of a plasma frequency and its doping dependence are already

https://doi.org/10.1021/acs.jpcc.1c07567
J. Phys. Chem. C 2022, 126, 1881−1889

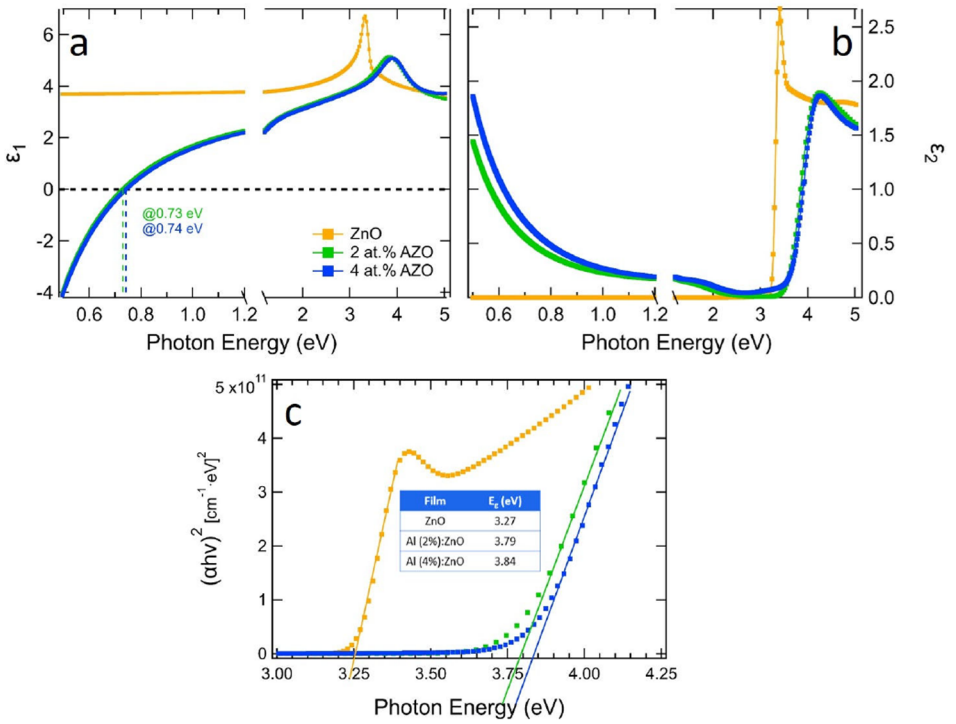

Figure 4. Real (a) and imaginary (b) part of the dielectric function of AZO films of different doping levels (2 and 4 at. %) as extracted by ellipsometry measurements. Measurements on a ZnO film (orange lines) are reported for reference. The dashed lines in ε_1 indicate the plasma frequency for 2 at. % AZO (green) and 4 at. % AZO (blue line). (c) Squared optical absorption coefficient versus photon energy for AZO films of different doping levels (2 and 4 at. %) as well as a ZnO film. The inset table shows the band gap values determined by a linear extrapolation along the absorption edge to the background.

qualitatively observable from the raw SE spectra. The thickness of the films corresponding to the best fit was 110 ± 10, 145 ± 15, and 145 ± 15 nm for Al-doped ZnO films (2 and 4 at. %, respectively), while the effective optical roughness was found to be approximately 4.0 ± 0.1 nm for ZnO, 6.0 ± 0.1 nm for the 2 at. % AZO film, and 4.6 ± 0.2 nm for the 4 at. % AZO film. We notice that whereas the mathematical uncertainty in thickness from the fit was very small (±0.1 nm), there are other sources of uncertainty (e.g., slight thickness inhomogeneities) that concur in defining a "physical" uncertainty that is larger than the "mathematical" uncertainty of the fit. The slightly different roughness values deduced by SE and AFM are typical of the different lateral scale over which the two techniques assess the sample and of the "effective" nature of roughness modeling in SE.

From the so-called Drude dielectric function (eq 1) and the definition of plasma frequency (eq 2), it is possible to calculate the density of the free carriers, N_e.

$$\varepsilon_{\text{Drude}} = \varepsilon_1 + i\varepsilon_2 = \varepsilon_\infty - \frac{\omega_p^2}{\omega^2 + i\gamma\omega} \quad (1)$$

$$\omega_p = \sqrt{\frac{N_e q^2}{m^* \varepsilon_0}} \quad (2)$$

In eq 1, ε_∞ is the background permittivity and ω is the photon frequency, while ω_p is the plasma frequency and γ the damping parameter. In eq 2, ε_0 is the vacuum permittivity, q is the elementary charge, and m^* is the effective mass of the charge carriers (for AZO $m^* = 0.27m_e$[59]). The calculated values of the carrier density of the corresponding films (2 and 4 at. % AZO) were 2.98 × 10^{20} and 3.91 × 10^{20} cm^{-3} (see Figure S5), respectively, which point out the higher conductivity of the 4 at. % AZO film, as expected,[48,49] and they are in good agreement with literature values.[60,61]

3.2. Optical Properties of Au Nanoparticles on AZO Films. The SE spectra of the Au−NP/AZO system are reported in Figure 5. In the same graph, we report the bare-substrate spectra for the sake of comparison. The SE spectra of the Au NPs/TCOs in different angles of incidence along with the fit curves are shown in Figure S6. The SE spectra of the hybrid system are different with respect to their bare counterpart due to the introduction of an additional dispersive layer on top of the system. A common feature of the SE spectra of Figure 5 seems to be the appearance of a peak around 2.1 eV in Ψ, intuitively related to the LSPR of Au NPs on top of the TCO surface (see also the transmission spectra of bare and NP-decorated AZO films reported in Figure S7, where a clear fingerprint of the LSPR is seen at that energy). By comparing the ellipsometry spectra of Au NPs on bare and Al-doped (2% and 4%) ZnO (Figure 5), we observe a slight blue-shift of such a structure as a function of increasing doping. We observe a slight decrease of the peak width as the doping of the TCO films is increased from 2% to 4% (Figure 5g). To shed more light on these observations, a dielectric modeling of the Au−NP/AZO system is required.

To fit the new spectra and extract the optical response of the Au−NP layer, the SE model was accordingly modified to include a new dielectric layer, representative of the effective dielectric function of an Au−NP assembly,[62,63] which was approximated as dielectrically isotropic.[64] Fits with MSE of 10.25, 6.82, and 25.55 for hybrid systems of Au NPs on top of bare and Al-doped (2 and 4 at. %) ZnO films were achieved,

https://doi.org/10.1021/acs.jpcc.1c07567
J. Phys. Chem. C 2022, 126, 1881−1889

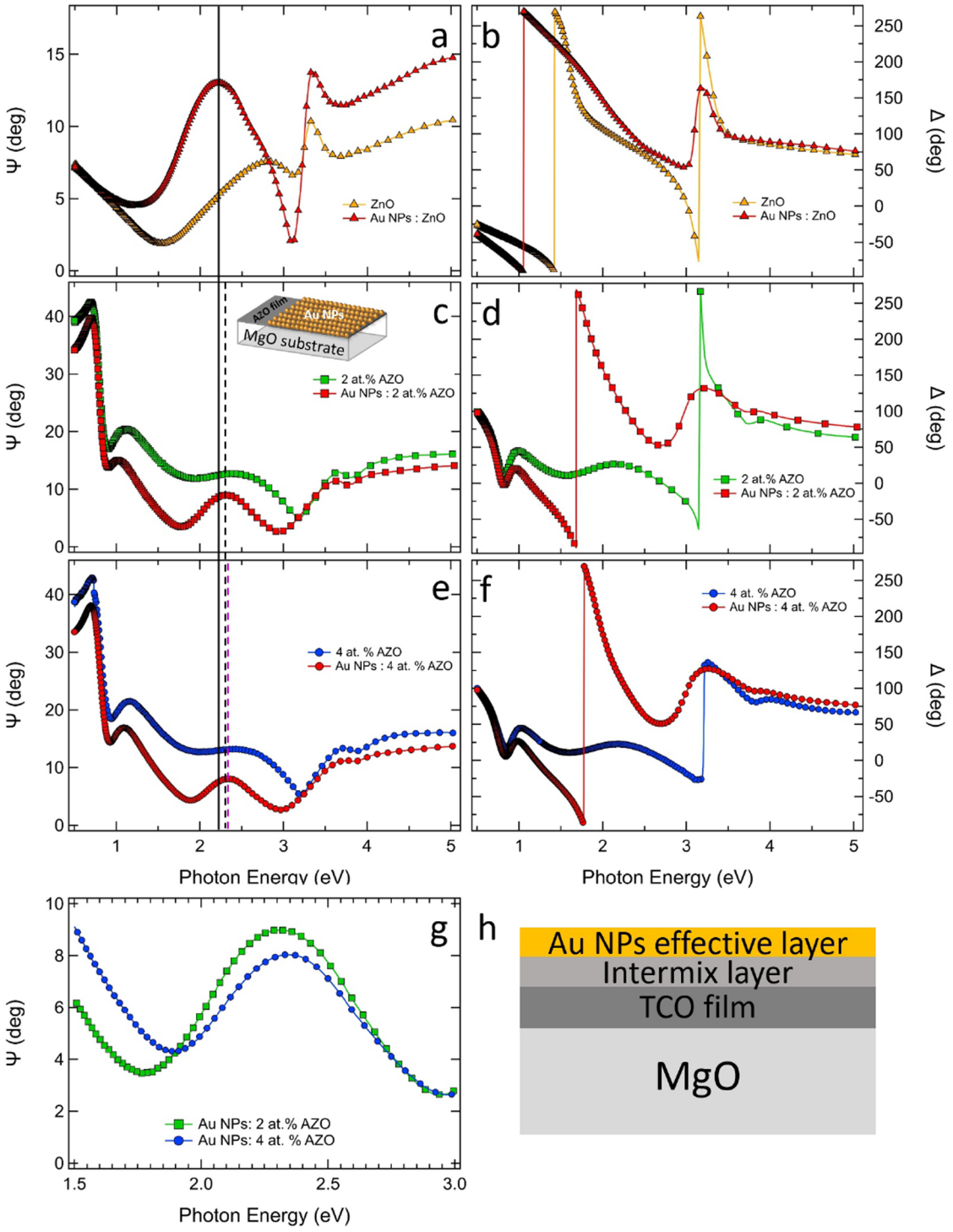

Figure 5. Ψ (left) and Δ (right) spectra of ZnO (a, b), Au NPs/2 at. % AZO (c, d), and Au NPs/4 at. % AZO (e, f) films, with and without Au NPs on top, acquired with incidence angle of 65°. In all spectra, the red markers represent the data of the Au NPs−TCO system. Three lines were placed on the Ψ spectra to point out the peak, related to LSPR of Au NPs. The solid line was set at the peak of ZnO spectrum while the dashed lines indicate the peaks of Au NPs/2 at. % AZO (black dashed line) and Au NPs/4 at. % AZO (purple dashed line) spectra. (g) Ψ spectra of Au NPs/2 at. % AZO (squares) and Au NPs/4 at. % AZO (circles) films, acquired with incidence angle of 65°. Inset in (c): a representative scheme of the samples under study (Au NPs/AZO film/MgO substrate one side polished). (h) A representative scheme of the model used for the fit of the experimental ellipsometry data.

respectively. Figure 6 reports the refractive index n (a) and extinction coefficient k (b) of the effective Au−NP layer on bare ZnO and AZO films (2 and 4 at. %), grown on MgO substrates, as extracted from the real (ε_1) and imaginary (ε_2) part of the dielectric function, corresponding to the best fit (Figure S8).

The extinction coefficient, k, of the Au−NP layer, extracted via the best fitting of the SE spectra, shows a resonance at 2.06

https://doi.org/10.1021/acs.jpcc.1c07567
J. Phys. Chem. C 2022, 126, 1881−1889

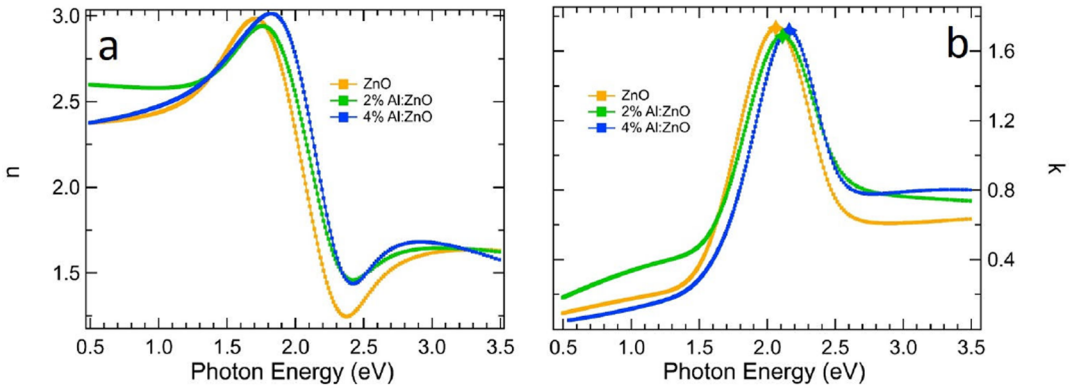

Figure 6. Refractive index, n (a). and extinction coefficient, k (b), of the effective Au-NP layer on bare ZnO and AZO films (2% and 4%), as extracted by spectroscopic ellipsometry. Markers on the k peak were placed for the sake of clarity of the LSPR blue-shift.

eV for Au on ZnO, 2.11 eV for Au on 2 at. % AZO, and 2.16 eV for Au on 4 at. % AZO. This resonance, the spectral fingerprint of the LSPR of Au NPs, exhibits a clear blue-shift as a function of increased doping of the TCO film, as actually observed in the raw SE data. We point out that the effective dielectric function of the Au−NP layer extracted from SE also allows to reproduce, with very minor changes, the transmission data (see e.g. the case of Au NPs/2 at. % AZO reported in Figure S9), thereby supporting the analysis results.

At this point, it is worth mentioning that there is rather conclusive evidence that the NPs formed on top of the TCOs are separated into islands. If the Au atoms still formed a continuous film, we would not witness the presence of a LSPR in the optical data (both transmission and ellipsometry). The optical properties would be completely different with respect to our observations, whereas for the electronic properties a conductive layer would be formed on top of the AZO, contributing to the overall conductivity of the system.

In Figure 6b, a decrease of Au plasmon line width is confirmed going from 2% to 4% samples. We ascribe this phenomenon to the lower dissipation in the substrate in correspondence of the LSPR of 4%-doped AZO.

The evolution of the LSPR on the differently doped substrates can originate from a variety of effects. The size and shape of the particles are one such effect, but because AFM images provide no clear-cut evidence of a systematic variation of these parameters, we are inclined to rule them out. As a matter of fact, the mean radius of Au NPs on top of bare and Al-doped (2% and 4%) ZnO films as extracted from AFM images analysis was found to be 10.9 ± 0.2, 11.1 ± 0.2, and 10.6 ± 0.2 nm, respectively. Because of this analysis, no size trend is observed, so the LSPR shift cannot directly stem from these variations in size. Moreover, the mean radius of the NPs lies in a size range where the size dependence of the LSPR is extremely weak,[65] meaning that the shift in LSPR cannot be attributed to the small variations in the NPs size. Next, we consider the effect of particle environment, i.e., the interactions with the substrate, dividing them in two categories, namely the purely "dielectric" interactions (shift of the LSPR due to the different polarizability of the surrounding material) and electronic interactions, i.e., that imply a transfer of charge between the materials.

In a simple approximation, for a given metal NP with fixed size and shape, there is a linear relation connecting the dielectric constant of the environment at the resonance frequency and the LSPR frequency.[66] In our case, this is only qualitatively verified: indeed, the blue-shift of the LSPR when going from ZnO to 2%-doped AZO can be rationalized based on the corresponding decrease of ε_1 of the substrate in the spectral region of the LSPR. However, when going from the 2%-doped AZO to the 4%-doped AZO, we observe a further blue-shift not motivated by a corresponding variation of the dielectric function.

An appealing hypothesis for this is related to the occurrence of a charge transfer between the two materials. Hot electrons play a role in several hybrid systems that include plasmonic materials. On this basis, we cannot rule out their influence on our observations, even though we do not have the possibility to single them out. In general, however, we understand our observations in terms of a net transfer of electrons toward the Au NPs. Indeed, the increase of chemical potential in the AZO due to the doping may promote a charge accumulation in the Au NPs, which would lead to a blue-shift of the LSPR even in the absence of concomitant effects (shape, size, and dielectric environment). Taking into account the work function of bare and Al-doped (2 and 4 at. %) ZnO as extracted from ultraviolet photoelectron spectroscopy measurements (3.96, 4.17, and 4.51 eV, respectively) and knowing that the work function of gold is 5.3 eV, because ZnO is an n-type semiconductor we could assume that the contact between Au NPs and ZnO is a Schottky contact.[67] However, the difference between the work functions of gold and doped ZnO films is relatively small. Furthermore, the presence of occupied states at the Fermi level and the ability in screening charges in the conductive AZO have shown several times an Ohmic contact.[68] Therefore, distinguishing the type of metal/semiconductor junction cannot be accomplished just by knowing the work function of the materials involved because the role of the interface as well as the presence of defects can affect the type of contact.[69,70] Assuming that charge injection from the AZO substrate to the Au NPs is responsible for the blue-shift of the plasmon resonance, according to our calculations the relative variations of the carrier density of gold corresponding to a plasmon resonance shift from 2.06 eV to 2.11 and 2.16 eV should be 3.3×10^{21} and 6.7×10^{21} cm^{-3}, respectively. Considering that the Au coverage corresponds to a nominal 3 nm thickness, this leads to an average transferred charge to the NPs of about 0.05 and 0.11 e/atom for 2 and 4 at. % AZO films, respectively. These values are consistent, in absolute value, to what happens in other metal NPs/ZnO[71,72] and similar Au NPs/oxide systems[73,74] and can be sustained by the substrate due to the small volume of Au NPs with respect to

https://doi.org/10.1021/acs.jpcc.1c07567
J. Phys. Chem. C 2022, 126, 1881−1889

the film volume. Increasing further the dopant concentration above the optimal doping condition (4 at. %) introduces Al in interstitial sites, depopulation of the conduction band, and new defect states in the band gap.[48,49] The larger degree of complexity would in turn make it more difficult to understand and model charge transfer phenomena at the interface. This clearly represents an upper limit, assuming the doping-dependent variation of the polarizability of the substrate plays no role in the blue-shift. It is possible that both effects play a concomitant role in determining the actual value of LSPR shift. In this respect, we speculate that in analogous systems with a higher ratio between Au NP volume and TCO volume some of these effects could reflect on a variation of the optical response of the substrate following the deposition of plasmonic particles, promoting an intertwinned TCO/NPs relationship, which can potentially be exploited to tailor the ENZ regime as well.

4. CONCLUSIONS

In conclusion, we reported a spectroscopic ellipsometry investigation of the dependence of the LSPR of metallic NPs on the doping of a TCO film (here, Al-doped ZnO films). We investigated first the evolution of the dielectric properties of the substrate as a function of Al doping, recording an increase of the TCO band gap as a function of increasing doping due to the Moss−Burstein effect, and the appearance of Drude tail distribution due to the presence of free carriers. In addition, we showed that the LSPR of Au NPs deposited on the TCO blue-shifted as a function of increasing doping. Such a blue-shift cannot be simply understood in terms of a variation of the dielectric environment of the plasmonic nanoparticles; hence, we suggested that a doping-dependent charge transfer between the substrate and the NPs is responsible for the effect. This could have interesting implications in terms of either passively or actively tuning the optical response of hybrid plasmonic/TCO systems, exploitable for a broad range of energy/environmental applications, such as in light harvesting and photocatalytic devices.

■ ASSOCIATED CONTENT

Supporting Information

The Supporting Information is available free of charge at https://pubs.acs.org/doi/10.1021/acs.jpcc.1c07567.

AFM images of bare ZnO and AZO films of different doping levels, AFM images of Au NPs deposited on top of ZnO and AZO films, SEM and AFM images of reference ZnO films, ellipsometric spectra Ψ and Δ and optical properties of bare and Al-doped (2 and 4 at. %) ZnO films, ellipsometric spectra of the Au−NP layer deposited on top of ZnO and AZO films, transmission spectra of AZO/MgO and Au NPs/AZO films, modeling of the transmission measurements of Au NPs/AZO films and the extracted optical properties (PDF)

■ AUTHOR INFORMATION

Corresponding Author

Maria Sygletou − *OptMatLab, Dipartimento di Fisica, Università di Genova, I-16146 Genova, Italy;* orcid.org/0000-0002-7046-5001; Email: sygletou@fisica.unige.it

Authors

Stefania Benedetti − *CNR-Istituto Nanoscienze, 41125 Modena, Italy;* orcid.org/0000-0002-2683-4818

Alessandro di Bona − *CNR-Istituto Nanoscienze, 41125 Modena, Italy*

Maurizio Canepa − *OptMatLab, Dipartimento di Fisica, Università di Genova, I-16146 Genova, Italy;* orcid.org/0000-0002-5148-1233

Francesco Bisio − *CNR-SPIN, I-16152 Genova, Italy;* orcid.org/0000-0003-1776-3023

Complete contact information is available at: https://pubs.acs.org/10.1021/acs.jpcc.1c07567

Notes

The authors declare no competing financial interest.

■ ACKNOWLEDGMENTS

This project has received funding from the European Union's Horizon 2020 research and innovation programme under the Marie Skłodowska-Curie grant agreement no. 799126.

■ REFERENCES

(1) Ellmer, K. Past Achievements and Future Challenges in the Development of Optically Transparent Electrodes. *Nat. Photonics* **2012**, *6*, 809−817.

(2) Naghdi, S.; Rhee, K. Y.; Hui, D. C. W.; Park, S.-J. A Review of Conductive Metal Nanomaterials as Conductive, Transparent, and Flexible Coatings, Thin Films, and Conductive Fillers: Different Deposition Methods and Applications. *Coatings* **2018**, *8*, 278−304.

(3) Kang, E. S. H.; Shiran Chaharsoughi, M.; Rossi, S.; Jonsson, M. P. Hybrid plasmonic metasurfaces. *J. Appl. Phys.* **2019**, *126*, 140901.

(4) Gurung, S.; Anopchenko, A.; Bej, S.; Joyner, J.; Myers, J. D.; Frantz, J.; Lee, H. W. H. Atomic Layer Engineering of Epsilon-Near-Zero Ultrathin Films with Controllable Field Enhancement. *Advanced Materials Interfaces* **2020**, *7*, 2000844.

(5) Vezzoli, S.; Bruno, V.; DeVault, C.; Roger, T.; Shalaev, V. M.; Boltasseva, A.; Ferrera, M.; Clerici, M.; Dubietis, A.; Faccio, D. Optical Time Reversal from Time-Dependent Epsilon-Near-Zero Media. *Phys. Rev. Lett.* **2018**, *120*, 043902.

(6) Naik, G. V.; Liu, J.; Kildishev, A. V.; Shalaev, V. M.; Boltasseva, A. Demonstration of Al:ZnO as a plasmonic component for near-infrared metamaterials. *Proc. Natl. Acad. Sci. U. S. A.* **2012**, *109*, 8834−8838.

(7) Cao, W.; Li, J.; Chen, H.; Xue, J. Transparent electrodes for organic optoelectronic devices: a review. *J. Photonics Energy* **2014**, *4*, 040990.

(8) Babicheva, V. E.; Boltasseva, A.; Lavrinenko, A. V. Transparent conducting oxides for electro-optical plasmonic modulators. *Nanophotonics* **2015**, *4*, 165−185.

(9) Dondapati, H.; Santiago, K.; Pradhan, A. K. Influence of growth temperature on electrical, optical, and plasmonic properties of aluminum:zinc oxide films grown by radio frequency magnetron sputtering. *J. Appl. Phys.* **2013**, *114*, 143506.

(10) Kan, Z.; Wang, Z.; Firdaus, Y.; Babics, M.; Alshareef, H. N.; Beaujuge, P. M. Atomic-layer-deposited AZO outperforms ITO in high-efficiency polymer solar cells. *J. Mater. Chem. A* **2018**, *6*, 10176−10183.

(11) Tan, K. C.; Lee, Y. S.; Yap, S. L.; Kok, S. Y.; Nee, C. H.; Siew, W. O.; Tou, T. Y.; Yap, S. S. Pulsed laser deposition of Al-doped ZnO films on glass and polycarbonate. *J. Nanophotonics* **2014**, *8*, 084091.

(12) Gondoni, P.; Ghidelli, M.; Di Fonzo, F.; Carminati, M.; Russo, V.; Li Bassi, A.; Casari, C. S. Structure-dependent optical and electrical transport properties of nanostructured Al-doped ZnO. *Nanotechnology* **2012**, *23*, 365706.

(13) Li, Q. H.; Zhu, D.; Liu, W.; Liu, Y.; Ma, X. C. Optical properties of Al-doped ZnO thin films by ellipsometry. *Appl. Surf. Sci.* **2008**, *254*, 2922−2926.
(14) Zhai, C.-H.; Zhang, R.-J.; Chen, X.; Zheng, Y.-X.; Wang, S.; Liu, J.; Dai, N.; Chen, L.-Y. Effects of Al Doping on the Properties of ZnO Thin Films Deposited by Atomic Layer Deposition. *Nanoscale Res. Lett.* **2016**, *11*, 407−414.
(15) Pradhan, A. K.; Mundle, R.; Santiago, K.; Skuza, J.; Xiao, B.; Song, K.; Bahoura, M.; Cheaito, R.; Hopkins, P. Extreme tunability in aluminum doped Zinc Oxide plasmonic materials for near-infrared applications. *Sci. Rep.* **2015**, *4*, 6415.
(16) Zheng, H.; Zhang, R.-J.; Li, D.-H.; Chen, X.; Wang, S.-Y.; Zheng, Y.-X.; Li, M.-J.; Hu, Z.-G.; Dai, N.; Chen, L.-Y. Optical Properties of Al-Doped ZnO Films in the Infrared Region and Their Absorption Applications. *Nanoscale Res. Lett.* **2018**, *13*, 149−155.
(17) Qing-Geng, L.; Xiao-Yong, G.; Jin-Hua, G.; Yong-Sheng, C.; Shi-E, Y.; Jing-Xiao, L. Spectroscopic Ellipsometry Study on Surface Roughness and Optical Property of AZO Films Prepared by Direct-Current Magnetron Reactive Sputtering Method. *Chin. Phys. Lett.* **2008**, *25*, 4223−4226.
(18) Abb, M.; Albella, P.; Aizpurua, J.; Muskens, O. L. All−Optical Control of a Single Plasmonic Nanoantenna−ITO Hybrid. *Nano Lett.* **2011**, *11*, 2457−2463.
(19) Pau, J. L.; Abad, J. M.; Hernández, M. J.; Cervera, M.; Ruiz, E.; Nuñez, C.; Lorenzo, E.; Piqueras, J. Investigation of surface plasmon resonance in Au nanoparticles deposited on ZnO:Al thin films. Proceedings of the 8th Spanish Conference on Electron Devices, CDE'2011, 2011; pp 1−4.
(20) Chew, C. K. T.; Salcianu, C.; Bishop, P.; Carmalt, C. J.; Parkin, I. P. Functional thin film coatings incorporating gold nanoparticles in a transparent conducting fluorine doped tin oxide matrix. *J. Mater. Chem. C* **2015**, *3*, 1118−1125.
(21) Kravets, V. G.; Kabashin, A. V.; Barnes, W. L.; Grigorenko, A. N. Plasmonic Surface Lattice Resonances: A Review of Properties and Applications. *Chem. Rev.* **2018**, *118*, 5912−5951.
(22) Pelli Cresi, J. S.; Silvagni, E.; Bertoni, G.; Spadaro, M. C.; Benedetti, S.; Valeri, S.; D'Addato, S.; Luches, P. Optical and electronic properties of silver nanoparticles embedded in cerium oxide. *J. Chem. Phys.* **2020**, *152*, 114704.
(23) Kelly, K. L.; Coronado, E.; Zhao, L. L.; Schatz, G. C. The Optical Properties of Metal Nanoparticles: The Influence of Size, Shape, and Dielectric Environment. *J. Phys. Chem. B* **2003**, *107*, 668−677.
(24) Duval Malinsky, M.; Kelly, K. L.; Schatz, G. C.; Van Duyne, R. P. Nanosphere Lithography: Effect of Substrate on the Localized Surface Plasmon Resonance Spectrum of Silver Nanoparticles. *J. Phys. Chem. B* **2001**, *105*, 2343−2350.
(25) Bruno, V.; Devault, C.; Vezzoli, S.; Kudyshev, Z.; Huq, T.; Mignuzzi, S.; Jacassi, A.; Saha, S.; Shah, Y. D.; Maier, S. A.; et al. Negative Refraction in Time-Varying Strongly Coupled Plasmonic-Antenna−Epsilon-Near-Zero Systems. *Phys. Rev. Lett.* **2020**, *124*, 043902.
(26) Clavero, C. Plasmon-induced hot-electron generation at nanoparticle/metal-oxide interfaces for photovoltaic and photocatalytic devices. *Nat. Photonics* **2014**, *8*, 95−103.
(27) Kale, M. J.; Avanesian, T.; Christopher, P. Direct Photocatalysis by Plasmonic Nanostructures. *ACS Catal.* **2014**, *4*, 116−128.
(28) Kodiyath, R.; Manikandan, M.; Liu, L.; Ramesh, G. V.; Koyasu, S.; Miyauchi, M.; Sakuma, Y.; Tanabe, T.; Gunji, T.; Duy Dao, T.; Ueda, S.; Nagao, T.; Ye, J.; Abe, H. Visible-light photodecomposition of acetaldehyde by TiO_2-coated gold nanocages: plasmon-mediated hot electron transport via defect states. *Chem. Commun.* **2014**, *50*, 15553−15556.
(29) Pelli Cresi, J. S.; Spadaro, M. C.; D'Addato, S.; Valeri, S.; Benedetti, S.; Di Bona, A.; Catone, D.; Di Mario, L.; O'Keeffe, P.; Paladini, A.; Bertoni, G.; Luches, P. Highly efficient plasmon-mediated electron injection into cerium oxide from embedded silver nanoparticles. *Nanoscale* **2019**, *11*, 10282−10291.
(30) Schroeder, W. A.; Stark, T. S.; Smirl, A. L. Hot-carrier enhancement of photorefractive space-charge fields in zinc-blende semiconductors. *Opt. Lett.* **1991**, *16*, 989−991.
(31) Catchpole, K.; Polman, A. Plasmonic solar cells. *Opt. Express* **2008**, *16*, 21793−21800.
(32) Zhang, J.; Wu, Y.; Xing, M.; Leghari, S. A. K.; Sajjad, S. Development of modified N doped TiO_2 photocatalyst with metals, nonmetals and metal oxides. *Energy Environ. Sci.* **2010**, *3*, 715−726.
(33) Yang, G.; Jiang, Z.; Shi, H.; Xiao, T.; Yan, Z. Preparation of highly visible-light active N-doped TiO_2 photocatalyst. *J. Mater. Chem.* **2010**, *20*, 5301−5309.
(34) Abb, M.; Sepúlveda, B.; Chong, H. M. H.; Muskens, O. L. Transparent conducting oxides for active hybrid metamaterial devices. *J. Opt.* **2012**, *14*, 114007.
(35) Stratakis, E.; Kymakis, E. Nanoparticle-based plasmonic organic photovoltaic devices. *Mater. Today* **2013**, *16*, 133−146.
(36) Kumar, M.; Yun, J.; Kim, J. Metal/Semiconductor and Transparent Conductor/Semiconductor Heterojunctions in High Efficient Photoelectric Devices: Progress and Features. *Int. J. Photoenergy* **2014**, *2014*, 1−14.
(37) Sygletou, M.; Bisio, F.; Benedetti, S.; Torelli, P.; di Bona, A.; Petrov, A.; Canepa, M. Transparent conductive oxide-based architectures for the electrical modulation of the optical response: A spectroscopic ellipsometry study. *J. Vac. Sci. Technol. B* **2019**, *37*, 061209.
(38) Furube, A.; Hashimoto, S. Insight into plasmonic hot-electron transfer and plasmon molecular drive: new dimensions in energy conversion and nanofabrication. *NPG Asia Mater.* **2017**, *9*, e454.
(39) Kumar, S.; Sood, A. K. *Reviews in Plasmonics 2015*; Springer International Publishing: 2016; pp 131−167.
(40) Saavedra, J. R. M.; Asenjo-Garcia, A.; García de Abajo, F. J. Hot-Electron Dynamics and Thermalization in Small Metallic Nanoparticles. *ACS Photonics* **2016**, *3*, 1637−1646.
(41) Brongersma, M. L.; Halas, N. J.; Nordlander, P. Plasmon-induced hot carrier science and technology. *Nat. Nanotechnol.* **2015**, *10*, 25−34.
(42) Baffou, G.; Rigneault, H. Femtosecond-pulsed optical heating of gold nanoparticles. *Phys. Rev. B* **2011**, *84*, 035415.
(43) Liu, J. G.; Zhang, H.; Link, S.; Nordlander, P. Relaxation of Plasmon-Induced Hot Carriers. *ACS Photonics* **2018**, *5*, 2584−2595.
(44) Smith, K. J.; Cheng, Y.; Arinze, E. S.; Kim, N. E.; Bragg, A. E.; Thon, S. M. Dynamics of Energy Transfer in Large Plasmonic Aluminum Nanoparticles. *ACS Photonics* **2018**, *5*, 805−813.
(45) Ferrera, M.; Della Valle, G.; Sygletou, M.; Magnozzi, M.; Catone, D.; O'Keeffe, P.; Paladini, A.; Toschi, F.; Mattera, L.; Canepa, M.; Bisio, F. Thermometric Calibration of the Ultrafast Relaxation Dynamics in Plasmonic Au Nanoparticles. *ACS Photonics* **2020**, *7*, 959−966.
(46) Jun, Y. C.; Reno, J.; Ribaudo, T.; Shaner, E.; Greffet, J.-J.; Vassant, S.; Marquier, F.; Sinclair, M.; Brener, I. Epsilon-Near-Zero Strong Coupling in Metamaterial-Semiconductor Hybrid Structures. *Nano Lett.* **2013**, *13*, 5391−5396.
(47) Moss, T. S. The Interpretation of the Properties of Indium Antimonide. *Proc. Phys. Soc., B* **1954**, *67*, 775−782.
(48) Valenti, I.; Benedetti, S.; di Bona, A.; Lollobrigida, V.; Perucchi, A.; Di Pietro, P.; Lupi, S.; Valeri, S.; Torelli, P. Electrical, optical, and electronic properties of Al:ZnO films in a wide doping range. *J. Appl. Phys.* **2015**, *118*, 165304.
(49) Benedetti, S.; Valenti, I.; di Bona, A.; Vinai, G.; Castan-Guerrero, C.; Valeri, S.; Catellani, A.; Ruini, A.; Torelli, P.; Calzolari, A. Spectroscopic identification of the chemical interplay between defects and dopants in Al-doped ZnO. *Phys. Chem. Chem. Phys.* **2017**, *19*, 29364−29371.
(50) Wang, Y.; Chen, X.; Wang, L.; Yang, S.; Feng, Z. Properties of ZnO thin film on Al2O3 substrate prepared by pulsed laser deposition under different substrate temperature. *Phys. Procedia* **2011**, *18*, 85−90.

https://doi.org/10.1021/acs.jpcc.1c07567
J. Phys. Chem. C 2022, 126, 1881−1889

(51) Li, X. D.; Chen, T. P.; Liu, P.; Liu, Y.; Liu, Z.; Leong, K. C. A study on the evolution of dielectric function of ZnO thin films with decreasing film thickness. *J. Appl. Phys.* **2014**, *115*, 103512.
(52) Pal, D.; Mathur, A.; Singh, A.; Singhal, J.; Sengupta, A.; Dutta, S.; Zollner, S.; Chattopadhyay, S. Tunable optical properties in atomic layer deposition grown ZnO thin films. *J. Vac. Sci. Technol. A* **2017**, *35*, 01B108.
(53) Pal, D.; Mathur, A.; Singh, A.; Singhal, J.; Chattopadhyay, S. Photoluminescence of Atomic Layer Deposition Grown ZnO Nanostructures. *Materials Today: Proceedings* **2018**, *5*, 9965−9971.
(54) Bundesmann, C.; Ashkenov, N.; Schubert, M.; Rahm, A.; Wenckstern, H.; Kaidashev, E.; Lorenz, M.; Grundmann, M. Infrared dielectric functions and crystal orientation of a-plane ZnO thin films on r-plane sapphire determined by generalized ellipsometry. *Thin Solid Films* **2004**, *455*−*456*, 161−166.
(55) Toccafondi, C.; Uttiya, S.; Cavalleri, O.; Gemme, G.; Barborini, E.; Bisio, F.; Canepa, M. Optical properties of nanogranular and highly porous TiO_2thin films. *J. Phys. D: Appl. Phys.* **2014**, *47*, 485301.
(56) Herzinger, C.; Johs, B. *Guide to Using WVASE32*; J.A. Woollam Company: 1996.
(57) Herzinger, C. M.; Johs, B. D. Dielectric function parametric model, and method of use, 1998; https://www.freepatentsonline.com/5796983.html.
(58) Ferrera, M.; Magnozzi, M.; Bisio, F.; Canepa, M. Temperature-dependent permittivity of silver and implications for thermoplasmonics. *Phys. Rev. Materials* **2019**, *3*, 105201.
(59) Young, D. L.; Coutts, T. J.; Kaydanov, V. I.; Gilmore, A. S.; Mulligan, W. P. Direct measurement of density-of-states effective mass and scattering parameter in transparent conducting oxides using second-order transport phenomena. *Journal of Vacuum Science & Technology A* **2000**, *18*, 2978−2985.
(60) Lu, J. G.; Ye, Z. Z.; Zeng, Y. J.; Zhu, L. P.; Wang, L.; Yuan, J.; Zhao, B. H.; Liang, Q. L. Structural, optical, and electrical properties of (Zn,Al)O films over a wide range of compositions. *J. Appl. Phys.* **2006**, *100*, 073714−073714.
(61) Yang, W.; Liu, Z.; Peng, D.-L.; Zhang, F.; Huang, H.; Xie, Y.; Wu, Z. Room-temperature deposition of transparent conducting Al-doped ZnO films by RF magnetron sputtering method. *Appl. Surf. Sci.* **2009**, *255*, 5669−5673.
(62) Choy, T. C. *Effective Medium Theory: Principles and Applications*; International Series of Monographs on Physics; Clarendon Press: 1999.
(63) Decker, M.; Staude, I.; Pertsch, T.; Burger, S.; Petschulat, J.; Scharf, T.; Werdehausen, D. Using effective medium theories to design tailored nanocomposite materials for optical systems. *Current Developments in Lens Design and Optical Engineering XIX* **2018**, *10745*, 78−87.
(64) Anghinolfi, L.; Moroni, R.; Mattera, L.; Canepa, M.; Bisio, F. Flexible Tuning of Shape and Arrangement of Au Nanoparticles in 2-Dimensional Self-Organized Arrays: Morphology and Plasmonic Response. *J. Phys. Chem. C* **2011**, *115*, 14036−14043.
(65) Link, S.; El-Sayed, M. A. Size and Temperature Dependence of the Plasmon Absorption of Colloidal Gold Nanoparticles. *J. Phys. Chem. B* **1999**, *103*, 4212−4217.
(66) Noguez, C. Surface Plasmons on Metal Nanoparticles: The Influence of Shape and Physical Environment. *J. Phys. Chem. C* **2007**, *111*, 3806−3819.
(67) Catellani, A.; Calzolari, A.; Ruini, A. Effect of ultrathin gold on the Ohmic-to-Schottky transition in Al/ZnO contacts: A first-principles investigation. *J. Appl. Phys.* **2014**, *115*, 043711.
(68) Ahmadi, M.; Abrari, M.; Ghanaatshoar, M. An All-sputtered Photovoltaic Ultraviolet Photodetector Based on Co-doped CuCrO2 and Al-doped ZnO Heterojunction, 2021.
(69) Brillson, L. J.; Lu, Y. ZnO Schottky barriers and Ohmic contacts. *J. Appl. Phys.* **2011**, *109*, 121301.
(70) Özgür; Alivov, Y. I.; Liu, C.; Teke, A.; Reshchikov, M. A.; Doğan, S.; Avrutin, V.; Cho, S.-J.; Morkoç, H. A comprehensive review of ZnO materials and devices. *J. Appl. Phys.* **2005**, *98*, 041301.
(71) Benedetti, S.; Valenti, I.; Valeri, S.; Castilla, S.; Touzé, E.; Bronstein, Y.; Toumar, A.; Finocchi, F.; Lazzari, R. Polar Step-Driven Metal Nucleation and Growth: The Ag/ZnO($10\bar{1}0$) Case. *J. Phys. Chem. C* **2020**, *124*, 6130−6140.
(72) Chernysheva, E.; Srour, W.; Philippe, B.; Baris, B.; Chenot, S.; Duarte, R. F.; Gorgoi, M.; Cruguel, H.; Rensmo, H.; Montigaud, H.; Jupille, J.; Cabailh, G.; Grachev, S.; Lazzari, R. Band alignment at Ag/ZnO(0001) interfaces: A combined soft and hard x-ray photoemission study. *Phys. Rev. B* **2018**, *97*, 235430.
(73) Mitsuhara, K.; Kitsudo, Y.; Matsumoto, H.; Visikovskiy, A.; Takizawa, M.; Nishimura, T.; Akita, T.; Kido, Y. Electronic charge transfer between Au nano-particles and TiO_2-terminated SrTiO3-(001) substrate. *Surf. Sci.* **2010**, *604*, 548−554.
(74) Torelli, P.; Giordano, L.; Benedetti, S.; Luches, P.; Annese, E.; Valeri, S.; Pacchioni, G. X-ray Photoemission Study of the Charge State of Au Nanoparticles on Thin MgO/Fe(001) Films. *J. Phys. Chem. C* **2009**, *113*, 19957−19965.

https://doi.org/10.1021/acs.jpcc.1c07567
J. Phys. Chem. C 2022, 126, 1881−1889